PAPER

Check for updates

Flexible and adhesive liquid-free ionic conductive elastomers toward human–machine interaction†

Zhenyu Xu,[ab] Rui Li,[a] Huijing Li,[ab] Guorong Gao ✱[ab] and Tao Chen ✱[ab]

Based on the demand for flexible human–machine interaction devices, it is urgent to develop high-performance stretchable ionic conductive materials. However, most gel-based ionic conductive materials are composed of crosslinked polymer networks that contain liquids, and suffer from limitations of solvent volatilization and leakage, and the cross-linking restricts the movement and diffusion of polymer chains, making it difficult for them to achieve adhesion. Here, we introduce flexible and adhesive liquid-free ionic conductive elastomers (ICE) with salt using a non-crosslinked polymer strategy. The ICE show a transparency of 89.5%, T_g of −51.2 °C, negligible weight loss at 200 °C, a tensile fracture strain of 289.5%, and an initial modulus of 45.7 kPa, and is adhesive to various solid surfaces with an interfacial toughness of 11.4 to 41.4 J m^{-2}. Moreover, the ICE exhibit stable electrical conductivity under ambient conditions. Triboelectric nanogenerators (TENGs) were assembled on an electrical shell surface with the adhesive ICE as an electrostatic induction layer and were displayed for use as human–machine interactive keyboards. This approach opens a route to making adhesive and stable polymer ionic conductors for human–machine interaction.

1 Introduction

With the rapid development of human–machine interaction technology, there is an urgent need for the development of flexible stretchable electronic materials.[1,2] In the early stage, flexible elastic conductive materials were mainly polymer composites that were filled with metals, carbons, and conjugated polymers.[3,4] It was hard for them to achieve transparency and high conductivity at the same time. Recently, ionic conductors that conduct electricity using ions, including hydrogels[5] and ionic liquid gels,[6] have attracted wide research interest. These materials are composed of stretchable polymer networks and absorbed with aqueous electrolytes or ionic liquids, allowing a broad range of applications. The combination of conductivity,[7] stretchability,[8] transparency,[8] adhesiveness,[9,10] and self-healing[11] properties makes them ideal materials for ionotronic devices, including artificial skins,[12–14] artificial axons,[15] artificial muscles,[16] artificial tongues,[17] deformable touch panels,[18] generators,[19,20] and diodes.[21] However, these devices suffer from limitations inherent to the liquid-containing materials.

The hydrogels dehydrate rapidly under ambient conditions due to evaporation. By introducing hygroscopic components such as LiCl[22] and glycerin,[23] durable moisturizing hydrogels can be obtained, but their water contents vary significantly with temperature and humidity. A hydrogel sealed in a hydrophobic elastomer can keep its water content, but there is a hassle of interfacial separation[24,25] while ionic liquid gels suffer from liquid leakage upon deformation.[26] It is still urgent to develop ionic conductive materials with durability and stability for human–machine interactive devices.

More recently, ionic conductive elastomers (ICE) have been developed, which consist of polymer networks and mobile ions, but contain no liquid.[27–34] Because they are liquid-free, ICE have no weight or performance loss in air, thus achieving durability and performance stability that are extremely difficult or even impossible to realize by hydrogels and ionic liquid gels. Such advantages enable ICE to be demonstrated for making flexible and stable transistors,[35] sensors,[36] electroluminescent devices,[37] and triboelectric nanogenerators (TENGs).[38] In human–machine interaction scenarios, ICE are always integrated with machines or human bodies. However, chemical crosslinking restricts the movements of polymer segments, thereby preventing the continuous molecular interaction between polymers and the contacted substrates, thus making the ICE difficult to achieve adhesion. Therefore, it needs to be fixed to the target surface with glue or tape. A key challenge for an ICE ionotronic device toward human–machine interaction is to develop a liquid-free material system that combines

[a] Key Laboratory of Marine Materials and Related Technologies, Zhejiang Key Laboratory of Marine Materials and Protective Technologies, Ningbo Institute of Materials Technology and Engineering, Chinese Academy of Sciences, Ningbo 315201, China. E-mail: gaogr@nimte.ac.cn, tao.chen@nimte.ac.cn

[b] School of Chemical Sciences, University of Chinese Academy of Sciences, Beijing 100049, China

† Electronic supplementary information (ESI) available. See DOI: **https://doi.org/10.1039/d2sm00865c**

flexibility, self-adhesiveness, conductivity, transparency, high-temperature resistance, anti-drying, and anti-freezing.

In this study, we developed a novel flexible and adhesive liquid-free ICE toward human–machine interaction. The ICE are synthesized through a strategy of one-step free radical polymerization of liquid acrylate monomers containing dissolved solid lithium salts. The material is soft with an initial tensile modulus of 45.7 kPa and stretchable with a fracture strain of 289.5%. As the acrylate polymers are commonly used as adhesives due to the strong hydrogen bonding ability of ester groups,[39] the ICE generate adhesiveness to various solid substrates. We investigate the effects of lithium salt dosage and the type of polymer side group on the electrical conductivity and the obtained ICE with a maximum electrical conductivity of 1.8×10^{-2} S m^{-1}. The material also features optical transparency, high-temperature stability, as well as durability, and significantly higher decomposition voltage in comparison with hydrogels. We use the ICE to make strain sensors and stretchable TENGs. To demonstrate the advantages in the field of human–machine interaction, we use the flexibility and adhesion of the ICE to easily construct several TENGs on the electrical plastic shell, collect the voltage signals from TENGs, convert the signals into binary codes, and then convert them into letters and display them on a monitor.

2 Experimental section

2.1 Materials

2-Ethoxyethoxyethyl acrylate (EEEA) was obtained from J&K Scientific Co., Ltd. Ethylene glycol methyl ether acrylate (MEA), ethylene glycol phenyl ether acrylate (PEA), benzophenone (BP), lithium bis(trifluoromethanesulphonyl)imide (LiTFSI), acrylamide (AAm), N,N'-methylenebisacrylamide (MBAA), ammonium persulfate (APS) and N,N,N',N'-tetramethylethylenediamine (TEMED) were obtained from the Aladdin Shanghai Reagent Co., Ltd. Butyl acrylate (BA) was obtained from Shanghai Macklin Biochemical Co., Ltd. All chemicals were used as received. VHB™ 4905 tape (thickness 0.5 mm) was obtained from 3 M Corporation.

2.2 Synthesis of ionic conductive elastomers (ICE)

ICE were prepared by free radical polymerization of LiTFSI/acrylate monomer mixed solution under UV irradiation. A typical example is given below. LiTFSI (0.5 g, 1.7 mmol) and BP (0.005 g, 0.027 mmol) were added to the liquid monomer EEEA (4.82 g, 25.6 mmol). The mixture was stirred for 0.5 h to obtain a transparent solution. Then, the solution was poured into a mold composed of two quartz glasses and a silicone frame with an inner size of 60 mm × 60 mm × 1 mm, subsequently polymerized under UV light (365 nm) for 6 h to generate the PEEEA ICE.

2.3 Synthesis of the PAAm hydrogel ionic conductor

1.5 g AAm was dissolved in 1 M NaCl aqueous solution (10 mL) with 0.01 g MBAA as a cross-linker. APS (0.005 g) and TEMED (5 μL, 0.055 mmol) were added, subsequent by stirring for

10 min. The final solution was poured into a mold composed of two plate glasses and a silicone frame with a chamber size of 60 mm × 60 mm × 1 mm. The hydrogel was obtained after polymerizing at 40 °C for 6 h.

2.4 Material tests and characterizations

Differential scanning calorimetry (DSC). The DSC measurements were conducted on a NETZSCH DSC 214 machine with a temperature increase from −100 to 100 °C at a heating rate of 10 °C min^{-1}.

Thermogravimetric analysis (TGA). The TGA measurements were conducted on a PerkinElmer TGA 8000 machine with a temperature increase from 30 to 500 °C at a heating rate of 10 °C min^{-1} in an N$_2$ atmosphere.

Transmittance test. The optical transmittance of ICE (1 mm thickness) was measured on a PerkinElmer Lambda 950 UV/vis spectroscope in the wavelength range of 400–800 nm.

Measurement of conductivity. The ionic conductivity was studied by electrochemical impedance spectroscopy conducted on a CHI660E electrochemical workstation. The ICE sheet (25 mm × 8 mm × 1 mm) was sandwiched between two copper electrodes (25 mm in length and 8 mm in width). Sinusoidal voltage waves with an amplitude of 0.01 V and frequency varying from 0.1 to 10^5 Hz were applied. The measured real (Z') and imaginary parts (Z'') of impedance at different frequencies were recorded as a Nyquist plot. The intercept of the real part of the Nyquist plot was taken as the resistance (R) of the hydrogel. The conductivity (σ) was calculated from $\sigma = d/RA$, where d is the distance between the electrodes, and A represents the area of an electrode.

Tensile tests. Tensile and cyclic tensile tests were conducted on a Universal Testing System (Zwick Roell Z1.0). ICE strips (25 mm × 8 mm × 1 mm) with a crosshead distance of 15 mm were stretched at a constant speed of 50 mm min^{-1}. Tensile strain was calculated as $(l - l_0)/l_0 \times 100\%$, where l was the length and l_0 was the initial length. Tensile stress was defined as F/A_0, where F is the force, and A_0 is the initial cross-sectional area (= 8 mm^2). Initial modulus (E) was defined as the slope of the stress–strain curve in the range of 0–50%.

90° peeling tests. Peeling tests were performed on the Zwick Roell Z1.0 Testing System. The ICE samples were cut into 15 mm × 1 mm × 0.8 mm sizes using a laser cutting machine (KT-4060, Liaochenshi Ketai Laser Equipment Co., Ltd). An adherend was spread and fixed on the lower platform. One end of an ICE sample was clamped on the upper clamp. Before peeling, the initial ICE-adherend contact area was set at 15 mm × 0.8 mm. The peeling speed was 50 mm min^{-1}. Interfacial toughness is determined by dividing the plateau force by the width of the hydrogel. In some cases, there is no plateau force, the maximum force was used to calculate the interfacial toughness.

2.5 Preparation of strain sensors based on ICE

A strain sensor was made by connecting both ends of a PEEEA ICE strip (25 mm × 8 mm × 1 mm) with copper wires. It was mounted on a Universal Testing System (Zwick Roell Z1.0) and

stretched at 50 mm min^{-1}. The electrochemical workstation (CHI660E) was used to apply a constant voltage of 1 V on the sensor and record the current (I) over time (t). The relative resistance ($\Delta R/R_0$) was calculated from $\Delta R/R_0 = (R - R_0)/R_0 = I_0/I - 1$, where R_0 and I_0 represent the initial resistance and current, respectively.

2.6 Preparation of the TENG

The TENG was prepared by sandwiching a layer of PEEEA ICE (30 mm × 30 mm × 1 mm) between two VHB^{TM} 4905 elastomers and connecting to the ICE with a copper electrode. The output performances, including open-circuit voltage (V_{oc}), short-circuit current (I_{sc}), short-circuit charge quantity (Q_{sc}), and power density of a TENG were recorded on an electrometer (Keithley 6514).

2.7 Preparation of a human–machine interactive system

Five TENGs were connected to a Mini STM 32 demo board (Guangzhou Xingyi Electronic Technology Co., Ltd) *via* separate signal capture circuits. The demo board converted electrical signals into digital signals, which were encoded and converted into letters and symbols by the microcontroller.

3. Results and discussion

3.1 Design and physical properties of the ionic conductive elastomer (ICE)

To synthesize the ICE, the electrolyte salt powder lithium bis(trifluoromethane sulfonimide) (LiTFSI) and the initiator benzophenone (BP) were dissolved in the liquid monomer 2-ethoxyethoxyethyl acrylate (EEEA) (Fig. 1a) to form a transparent solution. The molar percentage of LiTFSI to EEEA was fixed at 6.6% (molar ratio, 1:15) unless otherwise stated. The ICE were then obtained by polymerization under ultraviolet light (365 nm) irradiation for 6 h (Fig. 1b). The ICE is highly transparent in the visible light region. As shown in Fig. 1c, a sample with a thickness of 1 mm showed an average transmittance of 89.5% in the wavelength range of 400–800 nm. The high transparency indicates the LiTFSI powders were thoroughly dissolved in the polymer matrix, and no phase separation occurred during polymerization.

The liquid-free ICE exhibits high thermal stability and a wide operating temperature window. From the TGA curve in Fig. 1d, the ICE shows a slight weight loss of 1.4% when the temperature increases from 30 to 200 °C. From the DSC curve in Fig. 1e, the ICE show a glass transition (T_g) temperature of −51.2 °C, above which the ICE are flexible elastomers. Thus, the operating temperature of ICE can range from −51.2 to 200 °C. The weight loss before 200 °C (Fig. 1d) may be related to the water evaporation from the ICE, as the Li$^+$ in the ICE have the hygroscopic ability.[40] In sharp contrast, the PAAm hydrogel ionic conductor showed 60.1% weight loss when the temperature reached 100 °C in thermogravimetric analysis (Fig. S1, ESI†). Furthermore, the ICE is quite stable at high temperature. When stored in an oven at 80 °C, the naked ICE remained 98% of the initial mass after 2 h, which almost unchanged after another 10 h (Fig. S2, ESI†).

The ICE possesses good stretchability, with a fracture strain of 289.5% ± 32.6%, fracture stress of 56 ± 8.9 kPa, and initial modulus (E) of 45.7 ± 4.8 kPa. Fig. 1f shows the typical tensile stress–strain curve of the ICE. It also shows good resilience. In ten consecutive cyclic tensile tests with a maximum tensile strain of 150%, the strain always recovered to 4% after unloading at each cycle (Fig. S3, ESI†). The effect of polymer side groups on the mechanical properties of the ICE were investigated. Different types of ICE were synthesized by replacing EEEA with monomer ethylene glycol phenyl ether acrylate (PEA), butyl acrylate (BA), and ethylene glycol methyl ether acrylate (MEA) (Fig. S4a, ESI†), respectively. Typical tensile stress–strain curves of PPEA, PBA, and PMEA ICE are shown in Fig. S4b (ESI†). The fracture strain was 96.5% ± 4.5%, 522.3% ± 45.1%, and 450.3% ± 20.5% for PPEA, PBA, and PMEA ICE, respectively (Fig. S4c, ESI†) while the fracture stress was 603.9 ± 16.9 kPa, 199.7 ± 13 kPa, and 152.8 ± 4 kPa (Fig. S4c, ESI†), and the E was 875.4 ± 70.2 kPa, 134.7 ± 9.3 kPa, and 129.1 ± 5.5 kPa for PPEA, PBA, and PMEA ICE, respectively (Fig. S4d, ESI†). These results suggest that the tensile properties of ICE can be regulated by side groups. Polymers with rigid side groups, such as benzene rings, will restrict the activity of chain segments, and improve the strength and modulus of the ICE. Increasing the repeat units (such as ethoxy) of flexible side groups will improve the flexibility of polymers, and lead to reduced strength and modulus of the ICE. These results were consistent with DSC analysis, and the T_g was −5, −39.9, and −40 °C for PPEA, PBA, and PMEA, respectively (Fig. S4e, ESI†).

3.2 Adhesion properties of the ICE

The ICE is adhesive to various solid materials. Fig. 2a shows that the ICE pieces adhere to a piece of glass, paper, ICE, VHB tape, PDMS, PMMA, aluminum (Al), Nylon, copper (Cu), and cotton fabric. These adherends are dangling from ICE without shedding. The adhesion properties were evaluated through 90° peeling-off tests (Fig. 2b). The interfacial toughness of ICE adhered to the glass, paper, ICE, VHB, PDMS, PMMA, Al, Nylon, Cu, and cotton fabric is 41.4 ± 2.8, 37.8 ± 2.2, 32.7 ± 2.7, 29.5 ± 0.9, 26 ± 3, 17.4 ± 1.8, 17.1 ± 0.2, 15.2 ± 0.9, 13.8 ± 1.6, and 11.4 ± 0.5 J m^{-2}, respectively (Fig. 2c).

Adhesion is a complicated physical and chemical process, and the adhesion strength depends on the chemical interactions between interfaces and surface topology. Polyacrylates are commonly used to make solvent-free pressure-sensitive adhesives.[39] The forces acting between surfaces of non-polar polyacrylates and adherends can be classified as van der Waals interactions, which drop to an insignificant magnitude when the distance between the two bodies is greater than 0.5 nm.[41] The oxygen atoms on ester and ether groups from PEEEA easily form hydrogen bonds with hydroxyl or amino groups from the adherends.[42] On the other hand, the adhesion properties are affected by chemical cross-linking, which restricts the movement of polymer chains. Our PEEEA ICE was synthesized without chemical cross-linkers, and thus the polymer chains can diffuse across the surface of the target substrate to generate intimate contact on a molecular scale.[43]
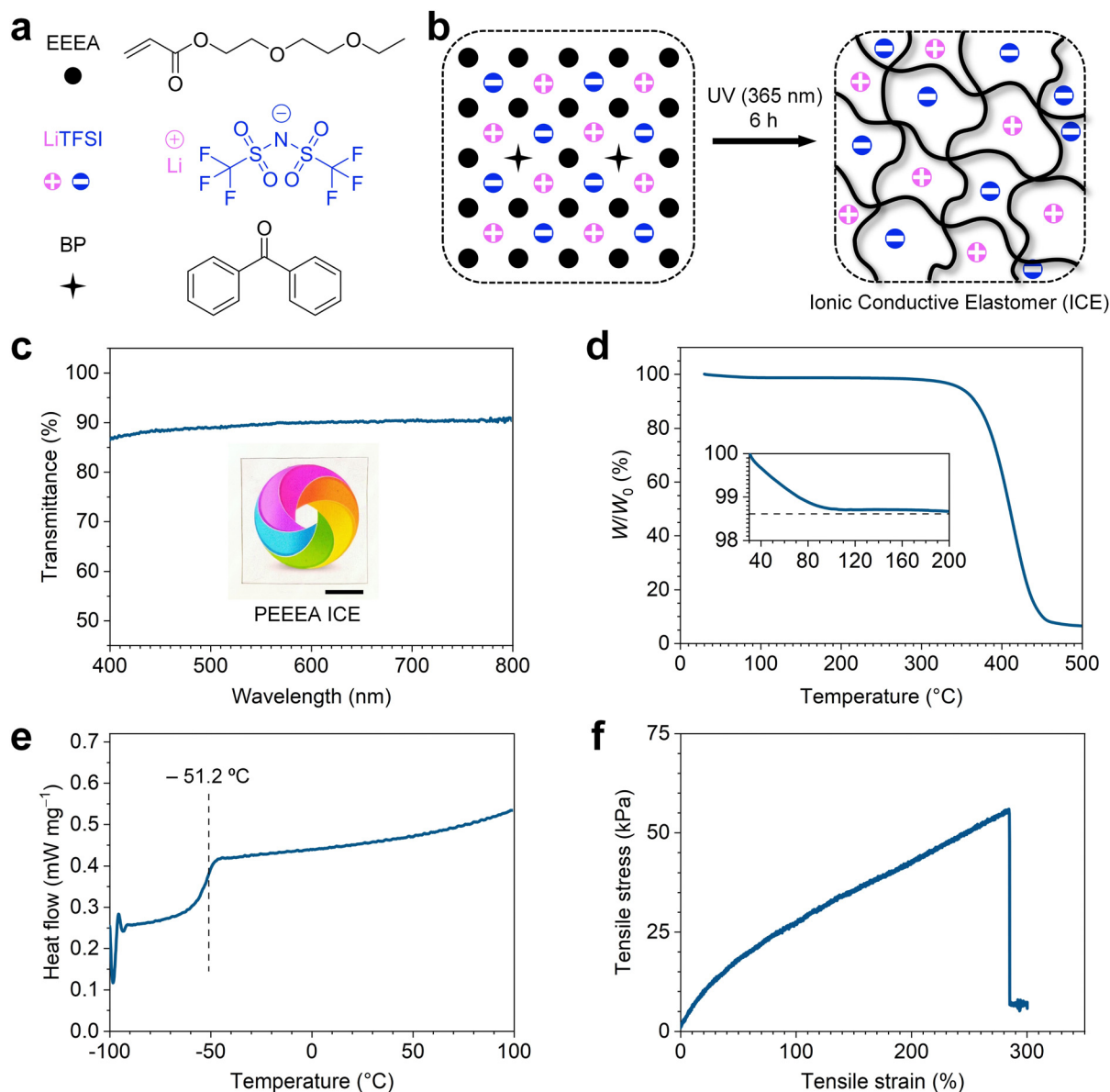
Fig. 1 Design and physical properties of the ionic conductive elastomer (ICE). Schematics illustrate (a) the molecular structures of EEEA, LiTFSI, and BP, and (b) the synthesis of ICE. (c) Transmittance spectra of the ICE. Inset photo showing the transparency of the material. Scale bar, 1 cm. (d) TGA curve, (e) DSC curve, and (f) tensile stress–strain curve of the ICE.

3.3 Electrical conductivity of the ICE

The ICE has good ionic conductivity. Fig. 3a shows the Nyquist plots of the ICE, which were prepared from various LiTFSI/monomer molar ratios. We calculated the conductivities (σ) by $\sigma = d/AR$, where d is equal to the thickness, A equal to the area of an ICE sample, and R is equal to the Z' value at the intersection point of the curve, and the Z' axis. The σ of the ICE with 4%, 6.6%, 13.3%, 19.9%, and 26.6% LiTFSI is $3.7 \times 10^{-3} \pm 1.6 \times 10^{-4}$, $5.7 \times 10^{-3} \pm 6.1 \times 10^{-4}$, $1.2 \times 10^{-2} \pm 1 \times 10^{-3}$, $1.8 \times 10^{-2} \pm 9.3 \times 10^{-4}$, and $1.4 \times 10^{-2} \pm 6.4 \times 10^{-4}$ S m^{-1}, respectively (Fig. 3b). The σ first increased by increasing the LiTFSI ratio, then decreased when exceeding 19.9%. We propose that the σ of the ICE is affected by the synergistic effects of

LiTFSI concentration and polymer segment motion ability. The mobile ions increase with the LiTFSI content, leading to the increase of σ. On the other hand, the coordination between Li$^+$ and carbonyl groups in polyacrylates reduces the flexibility of polymer chains.[44] It was confirmed by the linear rheological behavior of the PEEEA ICE and PEEEA polymer without LiTFSI (Fig. S5, ESI†). In a wide frequency range (0.1–100 Hz), the dynamic shear modulus, including storage modulus (G') and loss modulus (G'') of the PEEEA ICE are both significantly bigger than that of the PEEEA polymer. The combined effect is that the σ of the ICE reaches a maximum value when the molar ratio of LiTFSI to monomer is 19.9%. Moreover, with the same LiTFSI/monomer molar ratio of 6.6%, the σ sequence of three kinds of ICE is PPEA ($6 \times 10^{-6} \pm 4.3 \times 10^{-7}$) < PBA
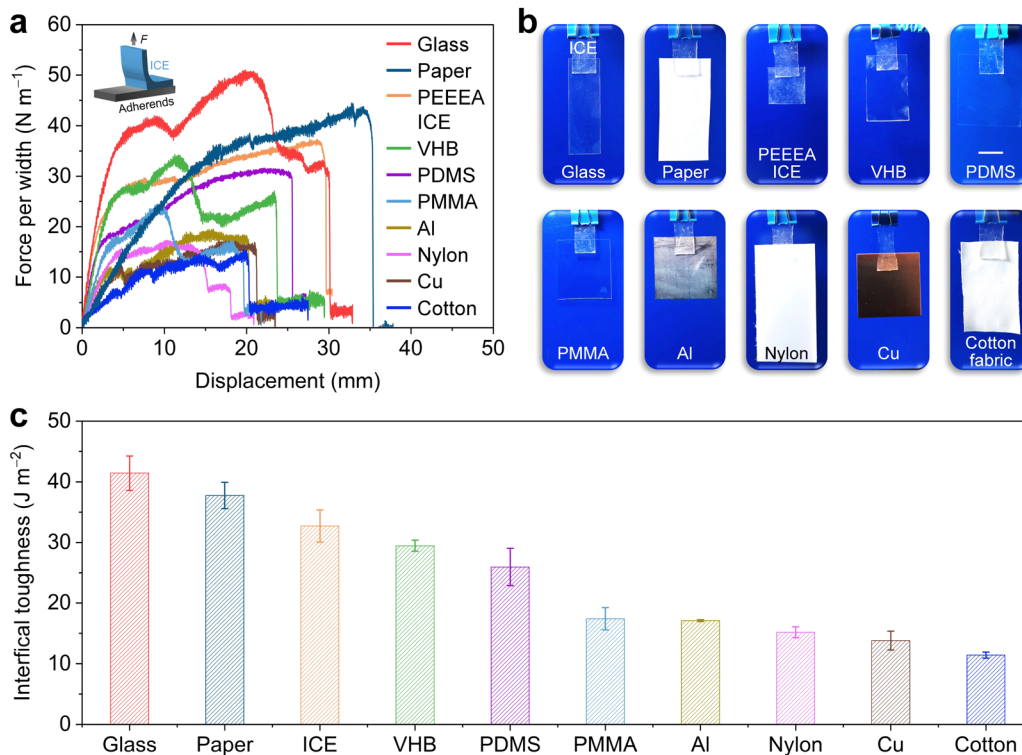
Fig. 2 Adhesion properties of the ICE. (a) Photos of various solid materials adhered to a piece of ICE. (b) 90° peeling-off tests and (c) corresponding interfacial toughness of the ICE adhered to the above materials.

$(5.3 \times 10^{-4} \pm 3.4 \times 10^{-5}) <$ PMEA ICE $(3.4 \times 10^{-3} \pm 8.16 \times 10^{-4})$ (Fig. S6, ESI†), which is consistent with the reverse order of T_g of these ICE (Fig. S4e, ESI†). These results prove that the σ of the ICE decreases with the reduction of polymer chain activity. The σ of the ICE increases monotonously with

increasing temperature (Fig. 3c), as higher temperature leads to greater chain activity thus facilitating ion mobility.

The ICE are stable in ambient conditions. Fig. 3d shows when being exposed to the atmosphere at room temperature, the σ of ICE decreased from 5.3×10^{-3} to 4.7×10^{-3} in the first

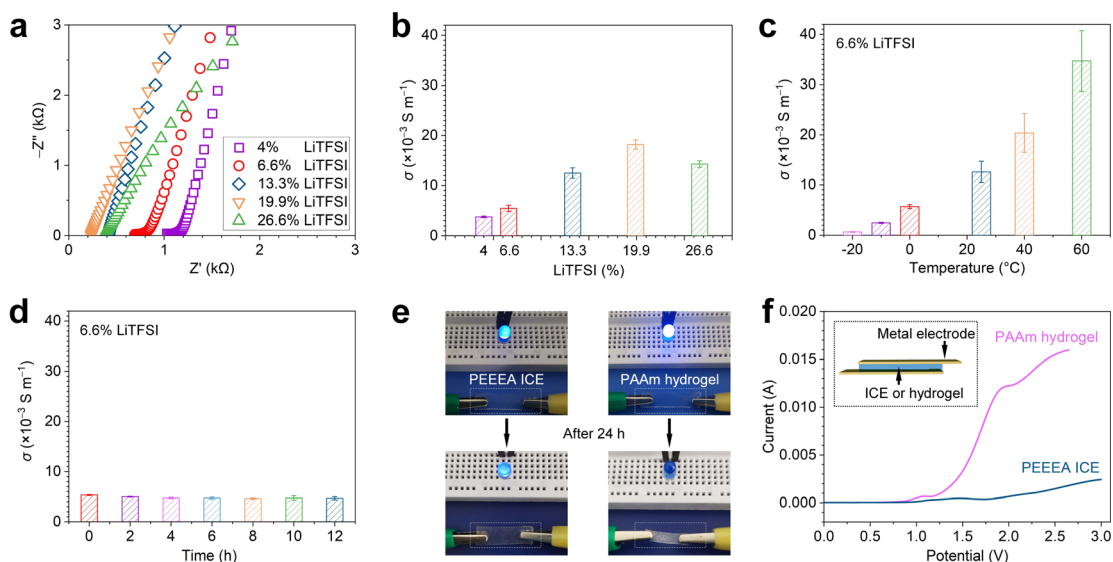**Fig. 3** Electrical conductivity of an ICE. (a) Nyquist plots of an ICE with various LiTFSI concentrations, and (b) corresponding conductivity (σ). (c) σ of the ICE with a constant LiTFSI concentration of 6.6% varies by temperature, and (d) varies by time in ambient conditions. (e) Photos show an LED light in a circuit with the ICE as the electric wire was bright, but an LED in a circuit with hydrogel as the electric wire dimmed after 24 h. (f) Linear sweep voltammetry curves of the hydrogel and the ICE.

4 h, probably due to the absorption of water from the air, and then remained at 4.7×10^{-3} until 12 h. When a piece of ICE was used as a wire in a direct current circuit, the indicator bulb remained bright after 24 h. In contrast, with an ionic hydrogel wire, the bright light bulb completely went out after 24 h. Fig. 3f shows the linear-sweep-voltammetry curves of ICE and PAAm hydrogel that conduct on a CHI660E electrochemical workstation, the scan rate was 1 mV S^{-1} at the range of 0–3 V. The curve of hydrogel rose steeply when voltage exceeded 0.8 V, indicating the electrolysis of water. The curve of ICE was flat until 1 V voltage, indicating that a higher voltage can be applied to the ICE. The resistances of the ICE samples increased by tensile (Fig. S7a, ESI†) or gradual tensile tests with a strain increment of 20% at each step (Fig. S7b, ESI†) when 1 V voltage was applied, and thus the ICE could be used as strain sensors.[3,4]

3.4 Mechanism and characterization of the stretchable ICE TENG

A single-electrode mode TENG is prepared with the ICE as the flexible interlayer electrode and VHB™ 4905 tape as the surface layer electrification material (Fig. 4a). Fig. 4b shows an ICE TENG stretched to a strain of 170%. The TENG produces

alternating current based on the coupling effect of contact electrification and electrostatic induction (Fig. 4c). Briefly, in step I of Fig. 4c, contact electrification occurs at the interface when a contact material, such as a Nylon plate, contacts the electrification layer, due to the difference in electron affinity between the two materials. In step II of Fig. 4c, as the Nylon plate moves away, the negative charges in the VHB layer induce the directed migration of the positive ions, thus electrons flow from the copper electrode to the ground, until an electrostatic equilibrium is established in step III of Fig. 4c. In step IV of Fig. 4c, as the Nylon plate turns back, electrons flow back from the ground. Thus, the alternating current is detected.

To evaluate the output performance of the TENG, a reciprocating motor with a Nylon plate at the top was used to provide contact-separation motion relative to an ICE TENG (size, 3 cm × 3 cm) at a frequency of 3 Hz. The peak open-circuit voltage (V_{oc}) is 98 V (Fig. 4d), the short-circuit charge quantity (Q_{sc}) is 32 nC (Fig. 4e), and the peak to peak short-circuit current (I_{sc}) is 1.8 µA (Fig. 4f). The output power density was further evaluated by varying the external resistance (R) (Fig. 4g). The voltage applied to the R increases, while the current in the circuit decreases as the R increases from 10^4 to
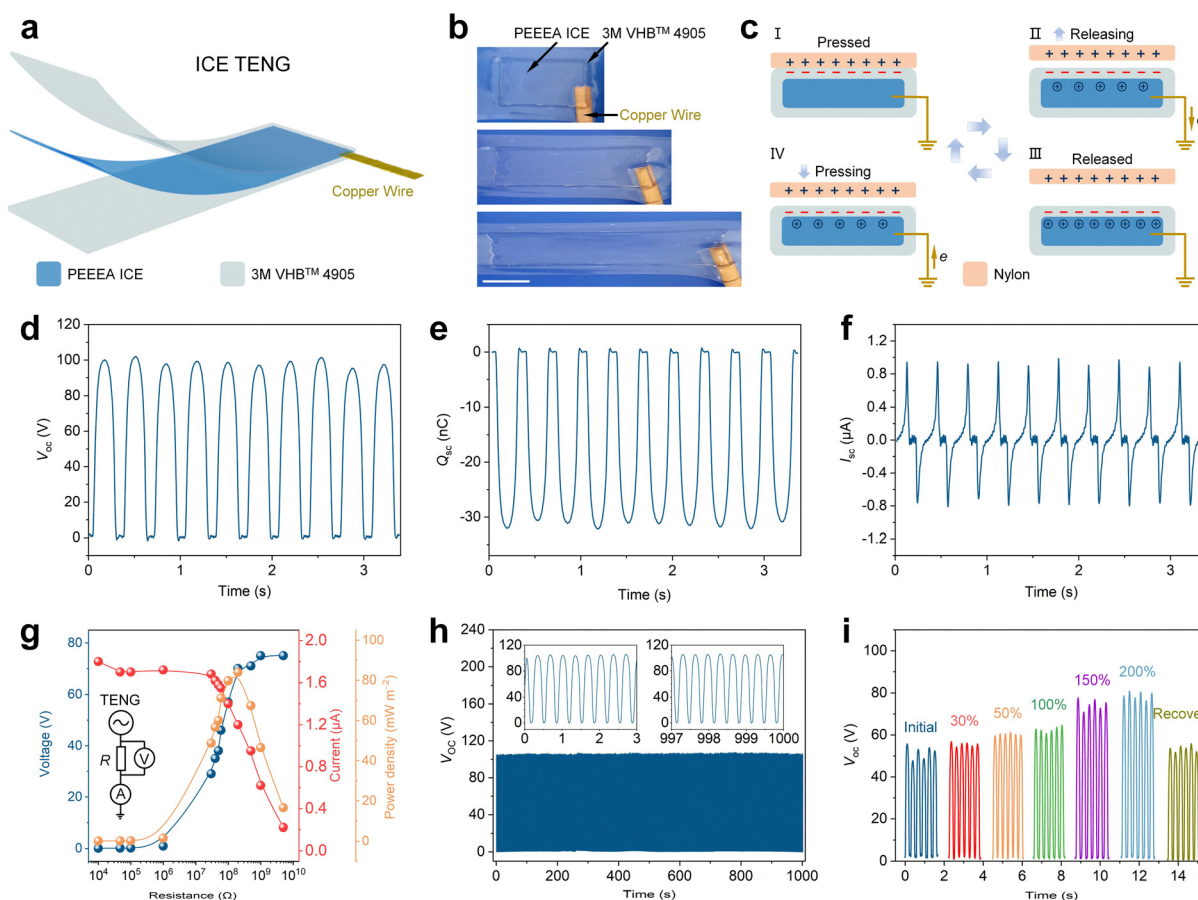

Fig. 4 Mechanism and characterization of the stretchable ICE TENG. (a) Schematic illustration of the architecture of TENG. (b) Photos show that a TENG was stretched to a strain of 170%. (c) The working mechanism of TENG. (d) The open–circuit voltage (V_{oc}), (e) short–circuit charge quantity (Q_{sc}), and (f) short–circuit current (I_{sc}) of an ICE TENG changed by time. (g) Variation of voltage, current, and power density on an external resistance. (h) The V_{oc} of a TENG in 3000 tapping cycles. (i) The V_{oc} of a TENG recorded at varied tensile strains.

5×10^9 Ω (Fig. 4g). The maximum power density is 84 mW m^{-2} at R of 200 MΩ. The durability of the ICE TENG is evaluated by tapping it for 3000 cycles. Fig. 4h shows the peak V_{oc} is almost unchanged at 102 V in the whole process. The ICE TENG could also generate electricity after stretching. A TENG with an initial size of 1 cm × 2 cm was stretched to 30%, 50%, 100%, 150%, 200%, then recovered to 0, the corresponding V_{oc} was 56, 61, 62.5, 76, 80 V, which then recovered to 52 V (Fig. 4i). The improvement of V_{oc} could be attributed to the increase in surface area of TENG, as the amounts of charges in the contact electrification step increase with the contact area.

3.5 Flexible and adhesive ICE-based TENG toward human–machine interaction

We developed a flexible and adhesive human–machine interaction system based on ICE TENG (Fig. 5a). Five TENGs were connected to five field-effect transistors (FETs), which are used as analog switches and were connected to a demo board through five circuits (Fig. 5a). When a finger tapped a TENG, a voltage pulse was generated (Fig. 5b), and thus the corresponding FET was turned on. The microcontroller unit (MCU) in the demo board can distinguish between tapping or no tapping of a TENG according to the corresponding FET. Defining

tapping as "1" and no tapping as "0", there are $2^5 - 1$ five-bit binary codes, from 00001 to 11111, which could be generated individually or simultaneously by tapping the five TENGs. We imparted each binary code a specific meaning, such as a letter, punctuation, or function key (Fig. 5c) that could be read from the monitor on the demo board (Fig. 5a), thus demonstrating the ICE TENG can be used as flexible and wearable human–machine interaction "keyboard". For example, "A" appeared on the monitor by tapping the fifth (ε, Fig. 5d) TENG, and "B" appeared by taping the fourth (δ, Movie S1, ESI†) TENG. Furthermore, we assembled the ICE TENG on an electrical plastic shell where the ICE was self-adhered to the curved shell, covered by PDMS films, and then connected with metal wires to form the TENG. Fig. 5e and Movie S2 (ESI†) show the typing of these TENG to input letters. To accommodate the novice, the MCU treated the signals within 1 s as simultaneous tapping.

4 Conclusions

In summary, we have reported a flexible and adhesive liquid-free ICE that consists of long PEEEA chains and LiTFSI that are dissolved in the polymer matrix. The material with a T_g of
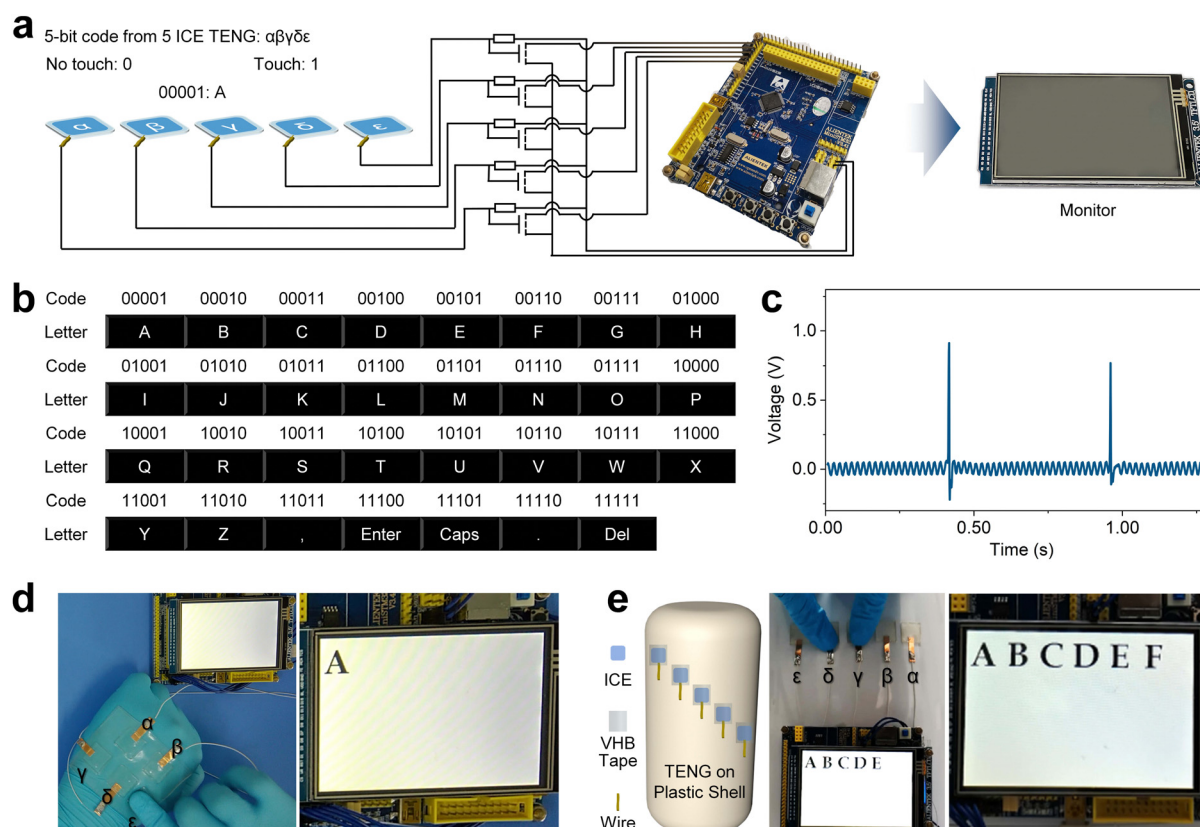

Fig. 5 Flexible and adhesive ICE-based TENG toward human–machine interaction. (a) A diagram shows a human–machine interactive system that consists of five TENGs, five signal acquisition circuits, a signal processing board, and a displayer. (b) Voltages are generated from the gentle tapping of a TENG by a latex gloved hand. (c) 5-bit binary codes corresponding to letters, punctuations, and function keys. (d) Photos show typing the letter "A" by touching the TENG wearing on hand, and (e) typing the letter "F" by touching the TENG that adhered to an electric shell. On the left is a schematic of the TENG assembled on an electronic plastic shell.

−51.2 °C and high-temperature stability shows a fracture strain of 289.5% and an initial modulus of 45.7 kPa. The ICE is adhesive to many solid substrates including plastics, rubbers, fabrics, metals, and glasses with interfacial toughness in the range of 11.4–41.4 J m^{-2}. The ICE can maintain the conductivity for long periods under ambient conditions, rather than losing the conductivity due to water loss as hydrogels. The ionic conductivity could be enhanced by increasing the LiTFSI concentration and the activity of polymer chains. We demonstrated the use of ICE to make TENGs, which were mechanically compliant and stretchable, and showed a V_{oc} of 98 V, Q_{sc} of 32 nC, I_{sc} of 1.8 μA, and a maximum power density of 84 mW m^{-2}. Flexible and adhesive TENGs were assembled on an electrical shell and were demonstrated to function as human–machine interactive "keyboards". The ICE provides possibilities for key flexible electronic devices and flexible human–machine interaction.

Conflicts of interest

There are no conflicts to declare.

Acknowledgements

References

1 P. Rothemund, Y. Kim, R. H. Heisser, X. Zhao, R. F. Shepherd and C. Keplinger, *Nat. Mater.*, 2021, **20**, 1582–1587.

2 Z. Xu, F. Zhou, H. Yan, G. Gao, H. Li, R. Li and T. Chen, *Nano Energy*, 2021, **90**, 106614.

3 H. Li, G. Gao, Z. Xu, D. Tang and T. Chen, *Macromol. Rapid Commun.*, 2021, **42**, 2100480.

4 H. Li, Y. Liang, G. Gao, S. Wei, Y. Jian, X. Le, W. Lu, Q. Liu, J. Zhang and T. Chen, *Chem. Eng. J.*, 2021, **415**, 128988.

5 S. Huang, L. Hou, T. Li, Y. Jiao and P. Wu, *Adv. Mater.*, 2022, **34**, 2110140.

6 W. Li, L. Li, S. Zheng, Z. Liu, X. Zou, Z. Sun, J. Guo and F. Yan, *Adv. Mater.*, 2022, **34**, 2203049.

7 C.-J. Lee, H. Wu, Y. Hu, M. Young, H. Wang, D. Lynch, F. Xu, H. Cong and G. Cheng, *ACS Appl. Mater. Interfaces*, 2018, **10**, 5845–5852.

8 C. Keplinger, J.-Y. Sun, C. C. Foo, P. Rothemund, G. M. Whitesides and Z. Suo, *Science*, 2013, **341**, 984–987.

9 Y. Miao, M. Xu, J. Yu and L. Zhang, *Sens. Actuators, B*, 2021, **327**, 128916.

10 Y. Miao, M. Xu and L. Zhang, *Adv. Mater.*, 2021, **33**, 2102308.

11 G. Gao, F. Yang, F. Zhou, J. He, W. Lu, P. Xiao, H. Yan, C. Pan, T. Chen and Z. L. Wang, *Adv. Mater.*, 2020, **32**, 2004290.

12 Z. Lei, W. Zhu, X. Zhang, X. Wang and P. Wu, *Adv. Funct. Mater.*, 2021, **31**, 2008020.

13 J. Wen, J. Tang, H. Ning, N. Hu, Y. Zhu, Y. Gong, C. Xu, Q. Zhao, X. Jiang, X. Hu, L. Lei, D. Wu and T. Huang, *Adv. Funct. Mater.*, 2021, **31**, 2011176.

14 I. You, D. G. Mackanic, N. Matsuhisa, J. Kang, J. Kwon, L. Beker, J. Mun, W. Suh, T. Y. Kim, J. B.-H. Tok, Z. Bao and U. Jeong, *Science*, 2020, **370**, 961–965.

15 D. Zhang, M. Zhang, J. Wang, H. Sun, H. Liu, L. Mi, C. Liu and C. Shen, *Adv. Compos. Hybrid Mater.*, 2022, DOI: **10.1007/s42114-022-00437-y**.

16 J. A. Rogers, *Science*, 2013, **341**, 968–969.

17 J. Yeom, A. Choe, S. Lim, Y. Lee, S. Na and H. Ko, *Sci. Adv.*, 2020, **6**, eaba5785.

18 C.-C. Kim, H.-H. Lee, K. H. Oh and J.-Y. Sun, *Science*, 2016, **353**, 682–687.

19 C.-G. Han, X. Qian, Q. Li, B. Deng, Y. Zhu, Z. Han, W. Zhang, W. Wang, S.-P. Feng, G. Chen and W. Liu, *Science*, 2020, **368**, 1091–1098.

20 R. Liu, Z. L. Wang, K. Fukuda and T. Someya, *Nat. Rev. Mater.*, 2022, DOI: **10.1038/s41578-022-00441-0**.

21 Y. Zhang, C. K. Jeong, J. Wang, X. Chen, K. H. Choi, L.-Q. Chen, W. Chen, Q. M. Zhang and Q. Wang, *Adv. Mater.*, 2021, **33**, 2103056.

22 Y. Bai, B. Chen, F. Xiang, J. Zhou, H. Wang and Z. Suo, *Appl. Phys. Lett.*, 2014, **105**, 151903.

23 F. Ni, N. Qiu, P. Xiao, C. Zhang, Y. Jian, Y. Liang, W. Xie, L. Yan and T. Chen, *Angew. Chem., Int. Ed.*, 2020, **59**, 19237–19246.

24 S. N. Subraveti and S. R. Raghavan, *ACS Appl. Mater. Interfaces*, 2021, **13**, 37645–37654.

25 Q. Liu, G. Nian, C. Yang, S. Qu and Z. Suo, *Nat. Commun.*, 2018, **9**, 846.

26 Z. Lei and P. Wu, *Nat. Commun.*, 2019, **10**, 3429.

27 B. B. Jing and C. M. Evans, *J. Am. Chem. Soc.*, 2019, **141**, 18932–18937.

28 P. Zhang, W. Guo, Z. H. Guo, Y. Ma, L. Gao, Z. Cong, X. J. Zhao, L. Qiao, X. Pu and Z. L. Wang, *Adv. Mater.*, 2021, **33**, 2101396.

29 P. Shi, Y. Wang, K. Wan, C. Zhang and T. Liu, *Adv. Funct. Mater.*, 2022, **32**, 2112293.

30 L. Wang, Y. Wang, S. Yang, X. Tao, Y. Zi and W. A. Daoud, *Nano Energy*, 2022, **91**, 106611.

31 K. Zhao, K. Zhang, R. A. Li, P. Sang, H. Hu and M. He, *J. Mater. Chem. A*, 2021, **9**, 23714–23721.

32 C. Dang, F. Peng, H. Liu, X. Feng, Y. Liu, S. Hu and H. Qi, *J. Mater. Chem. A*, 2021, **9**, 13115–13124.

33 X. Qu, W. Niu, R. Wang, Z. Li, Y. Guo, X. Liu and J. Sun, *Mater. Horiz.*, 2020, **7**, 2994–3004.

34 M. Wang, Z. Lai, X. Jin, T. Sun, H. Liu and H. Qi, *Adv. Funct. Mater.*, 2021, **31**, 2101957.

35 H. J. Kim, B. Chen, Z. Suo and R. C. Hayward, *Science*, 2020, **367**, 773–776.

36 L. Shi, T. Zhu, G. Gao, X. Zhang, W. Wei, W. Liu and S. Ding, *Nat. Commun.*, 2018, **9**, 2630.

37 J. Wang, C. Yan, G. Cai, M. Cui, A. Lee-Sie Eh and P. See Lee, *Adv. Mater.*, 2016, **28**, 4490–4496.

38 P. Zhang, Y. Chen, Z. H. Guo, W. Guo, X. Pu and Z. L. Wang, *Adv. Funct. Mater.*, 2020, **30**, 1909252.

39 Z. Czech and R. Milker, *J. Appl. Polym. Sci.*, 2003, **87**, 182–191.

40 S. Aleid, M. Wu, R. Li, W. Wang, C. Zhang, L. Zhang and P. Wang, *ACS Mater. Lett.*, 2022, **4**, 511–520.

41 M. D. Ellul, *THE ROLE OF DIFFUSION IN THE ADHESION OF ELASTOMERS (ADSORPTION, BUTYL RUBBER, VISCOELASTICITY)*, The University of Akron, 1984.

42 Y.-J. Wang, Y. He, S. Y. Zheng, Z. Xu, J. Li, Y. Zhao, L. Chen and W. Liu, *Adv. Funct. Mater.*, 2021, **31**, 2104296.

43 H. Yan, Y. Wang, W. Shen, F. Li, G. Gao, T. Zheng, Z. Xu, S. Qian, C.-Y. Chen, C. Zhang, G. Yang and T. Chen, *Adv. Funct. Mater.*, 2022, **32**, 2203241.

44 B. Yiming, Y. Han, Z. Han, X. Zhang, Y. Li, W. Lian, M. Zhang, J. Yin, T. Sun, Z. Wu, T. Li, J. Fu, Z. Jia and S. Qu, *Adv. Mater.*, 2021, **33**, 2006111.